

INFLUENCE OF ZONAL SURFACE ROUGHNESS ON THE CHARACTERISTIC CURVES OF A TURBOPUMP

B. Torner – F.-H. Wurm

Institute of Turbomachinery, Faculty of Mechanical Engineering and Marine Technology,
University of Rostock, Rostock, Germany

benjamin.torner@uni-rostock.de

ABSTRACT

The consideration of surface roughness in flow simulations of turbopumps can be an important factor in computing the pump characteristics (pressure head, efficiency) adequately. This is especially the case with radial turbopumps of low specific speeds, where dominant roughness effects can be present in the long, narrow blade channels and side chambers of the pump. These roughness effects must be accounted for in flow simulations. For this purpose, a roughness modeling is mostly used in flow solvers, for which an equivalent sand roughness k_s must be defined at the rough surface.

Regarding this, the present study investigates the roughness effects on the pump characteristics of a turbopump with different zonal roughnesses by a simulative approach. For this purpose, rough pump simulations were performed and the equivalent sand roughness k_s required for this purpose was determined beforehand using an in-house evaluation method. Then, the extent to which the different roughness regions have an influence on the pump characteristics was investigated in detail.

To carry out this procedure, it was first necessary to determine the equivalent sand roughnesses k_s at two locations of the pump – the impeller as well as the volute. For this purpose, the surface roughness at these walls were scanned and digitized. Subsequently, the specific equivalent sand roughness of the scanned surfaces was determined using rough channel flow simulations and an in-house evaluation method, which accounts for the roughness effects in the channel flow.

Afterwards, pump simulations were performed, using roughness modelling first in the volute and the front side chamber region. These simulations showed a significant reduction of head and efficiency compared to pump simulations with hydraulically smooth walls. Subsequently, an additional area in the impeller was defined as rough walls in the pump simulation. The additional roughness effects led to a further reduction of pump's efficiency along the whole performance curve, while the head did not decrease.

In conclusion, the study shows the importance of numerical consideration of rough walls in flow simulation of turbopumps with low specific speed. Significant discrepancies in pump characteristics can exist between experiments on a manufactured pump and flow simulations of a computer-designed pump if these roughnesses are not accounted for in the simulations.

KEYWORDS

Turbopump, Flow Simulation, Roughness Modelling, Zonal Roughness, Cast Iron, Discrete Porosity Method (DPM)

NOMENCLATURE

A	area, m ²	κ	constant, $\kappa = 0.41$
B	constant, $B = 5.0$	ν	kinematic viscosity, m ² /s
b	width, m	ρ	density, kg/m ³
c_D	drag coefficient, –	τ_w	wall shear stress, Pa
e_z	unit vector parallel to z-axis, –		
F_D	drag force, N		
H	channel height, m		
H_p	(total) pressure head, m		
H_s	static pressure head, m		
	$(p - \sum_{inlet} p \cdot \dot{m}_{cell} / \sum_{inlet} \dot{m}_{cell}) / \rho g$		
h	height, m		
k_a	average roughness height, m		
k_t	peak-to-trough roughness height, m		
k_s	equivalent sand grain roughness, m		
n	rotational speed, rpm		
n_A	unit vector parallel to dA , –		
n_q	specific speed, 1/min		
p	pressure, Pa		
Q	flow rate, m ³ /s		
r	radius, m		
Re_H	$u_b \cdot H / \nu$, –		
S	source term, Pa/m		
t_A	unit parallel vector, –		
u	velocity, m/s		
Δu^+	downshift due to the roughness, –		
V	volume, m ³		
x, y, z	directions, m		
α	area ratio, –		
δ_v	viscous boundary layer, m		
η_i	inner efficiency, %		

SUB-, SUPERSCRIPTS AND OPERATORS

b	bulk
$cell$	cell
H	channel height
i, j	spatial directions
$proj$	projected
t	total
Δ/d	increment
$+$	scaling with wall units
$\langle \dots \rangle$	time-averaged quantity

ABBREVIATIONS

BC	boundary conditions
CFD	computational fluid dynamic
EXP	experiment
SC	front side chamber
Rel. Dev.	relative deviation
URANS	Unsteady Reynolds-Averaged Navier-Stokes
2D	two-dimensional

INTRODUCTION

Turbopumps are used in many areas of application, such as industry, facility management or water and wastewater transport. These pumps account for a significant proportion of total energy consumption in Europe (1). Therefore, actions to analyze and increase efficiency are an important concern. Optimizations regarding efficiency can be done experimentally with the use of prototypes or numerically using CFD computations.

The pump optimization with CFD allows parameter studies to be carried out much more efficiently and leads usually to a result faster than experimental analyses. But the prerequisite for using numerical methods is that the models used in the optimization process represent reality to a sufficient degree. For CFD optimization in turbopumps, numerical methods are usually used which are based on the solution of the unsteady Reynolds-averaged Navier-Stokes equations (e.g., in Ref. (2)). In many of these CFD computations, the simulated results agree sufficiently well with measured values in the turbomachine, see for example Figure 1.

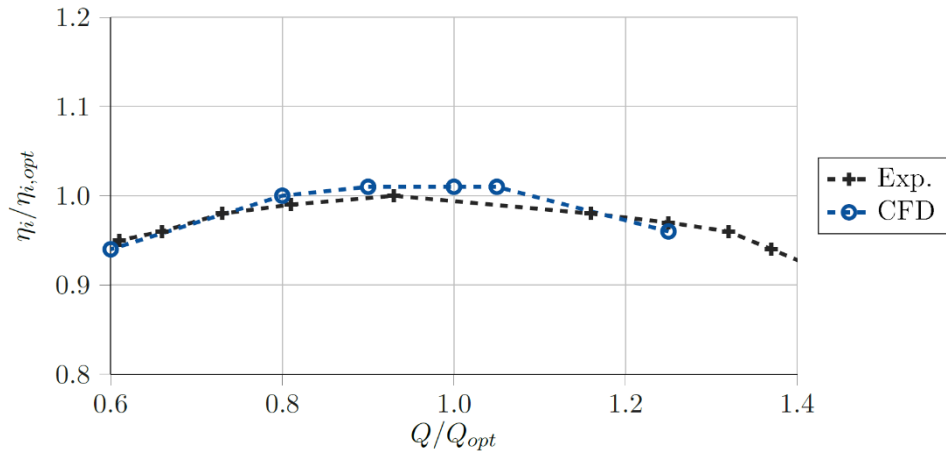


Figure 1: Efficiency curve of an industrial pump, $n_q > 15 \text{ min}^{-1}$. The figure bases on results in Ref. (5).

Nonetheless, for CFD computations in turbopumps with low specific speeds (n_q in the order of $8 - 15 \text{ min}^{-1}$), huge differences can exist in the pump characteristics between simulation and experiment, e.g., as shown in Figure 2. The specific speed n_q is defined by Ref. (1) as:

$$n_q = n \cdot \frac{Q^{1/2}}{H_p^{3/4}} \quad \{1\}$$

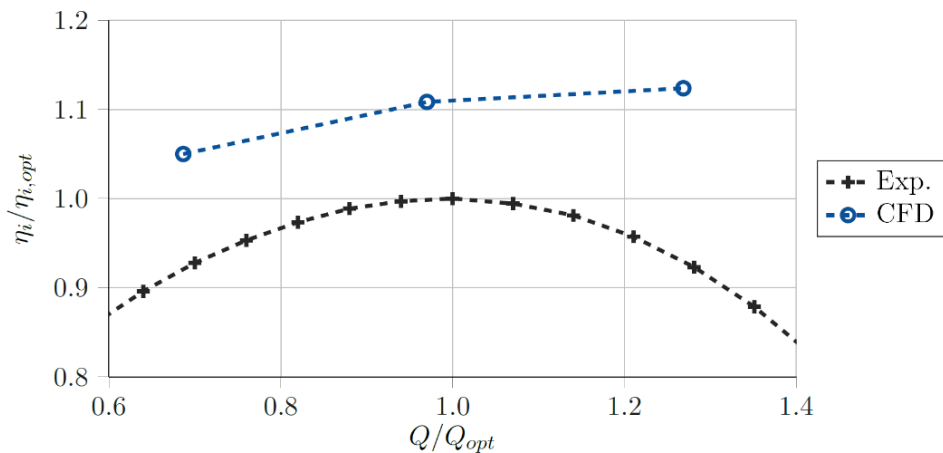


Figure 2: Efficiency curve of an industrial pump with low specific speed $n_q < 15 \text{ min}^{-1}$. The figure bases on results in Ref. (3).

The reasons for this were investigated in previous publications of the authors (3,4). The main reasons for the significant deviations between simulation and experiment were found in the inadequate modeling of roughness effects in the simulations and, in part, in the poor representation of a detachment at the volute's tongue. The latter problem could be solved by a special wall treatment in Ref. (5).

However, the consideration of roughness effects still poses a challenge for flow simulations in turbopumps. Usually, the equivalent sand roughness k_s is used for the consideration and modelling of the roughness effects in pump simulations (6–10). However, the determination of the equivalent sand roughness is complex, and literature indicates different results for comparable technical surfaces. This is also the case for cast iron, which is widely used for turbopump components.

Here, the literature indicates a range of equivalent sand roughnesses between $k_s = (130 - 3000) \mu\text{m}$ (1,11–14). This wide range is much too inaccurate to perform numerical simulations in turbopumps considering cast iron walls adequately. In addition, various pump parts were made of different materials (cast iron, investment casting) and could also be post-processed (e.g., polished). Hence, individual k_s -values should be specified in different pump parts.

For this reason, the purpose of this study is to analyze the effect of roughnesses on the simulated pump characteristics in a turbopump with low n_q by defining k_s specifically at individual surfaces. Therefore, the cast iron surfaces in two pump regions were scanned and digitized in a first step. Then, the k_s -value of the respective surfaces were determined by the help of rough channel flow simulations and an in-house evaluation method, the Discrete Porosity Method (DPM). By using the DPM, we were able to determine the specific k_s -values of an individual cast iron surface without directly resolving the roughness by the grid in the channel flow simulations. In a second step, these k_s -values were defined at the respective zonal wall regions (impeller, front side chamber, volute) in various turbopump simulations to determine the zonal roughness influence on the pump characteristics.

METHODS

Equivalent Sand Grain Roughness k_s

The first comprehensive flow investigations of roughness effects were made by Nikuradse (15) and Schlichting (16). In these studies, the velocity distribution and pressure drop in a turbulent channel flow with different surface roughnesses were analyzed. Based on the experimental results with sand of different grain size, Nikuradse derived similarity laws between smooth and rough surfaces. Later, Schlichting investigated artificial roughness and compared his results with those of Nikuradse. As a comparative value, he determined the sand grain size which produced the same friction loss as the artificial roughness. Since then, the equivalent sand roughness k_s has become established in fluid mechanics as a comparative value of the roughness effect.

The roughness influence on the flow can be determined from the ratio of equivalent sand roughness height k_s and the thickness of the viscous boundary layer $\delta_v = \nu / \sqrt{\tau_w / \rho}$. Therefore, the wall shear stress τ_w , the density ρ and the kinematic viscosity ν are considered to derive a dimensionless equivalent sand grain roughness k_s^+ :

$$k_s^+ = \frac{k_s}{\delta_v}. \quad \{2\}$$

With the limits given by Schlichting, the following subdivision of roughness flow regimes can be made: a wall flow is hydraulically smooth if the viscous boundary layer thickness is larger than the roughness elements ($k_s^+ < 5$), and transitional roughness prevails if the roughness elements partially protrude from the viscous boundary layer ($5 < k_s^+ < 70$). If all roughness elements of a surface are larger than the viscous boundary layer, it is called fully rough regime ($k_s^+ > 70$) (17). Based on previous results, it can be assumed that a transitional to fully rough regime exists in industrial pumps with low specific speed and cast iron walls (5).

With k_s and k_s^+ , the velocity profile of a fully developed flow near a rough wall can be described. First, the velocity profile for a smooth boundary layer in the logarithmic region is described by:

$$u^+ = \frac{1}{\kappa} \ln(y^+) + B. \quad \{3\}$$

Equation {3} is then extended and applies for rough walls with $\kappa = 0.41$ and $B = 5.0$:

$$u^+ = \frac{1}{\kappa} \ln(y^+) + B - \Delta u^+(k_s^+). \quad \{4\}$$

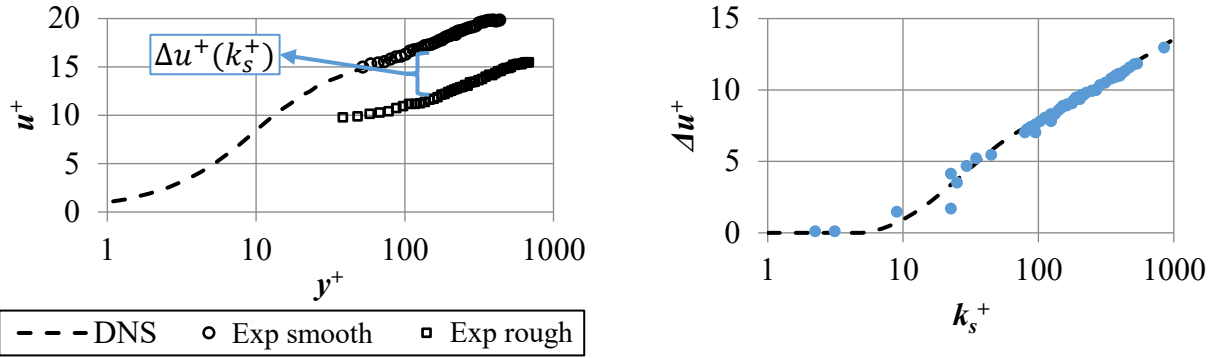


Figure 3: Left: Roughness influence on the velocity profile (data from Ref. (3)). Right: Roughness function $\Delta u^+ = f(k_s^+)$ based on the data of Ref. (18).

The velocity profile in the logarithmic region in a rough boundary layer deviates by a downshift Δu^+ from the profile in the smooth boundary. This downshift can be expressed by a roughness function $\Delta u^+ = f(k_s^+)$. Examples of velocity profiles and the course of the roughness function are given in Figure 3.

Discrete Porosity Method (DPM) for Computing Flows over Rough Walls

The Discrete Porosity Method (DPM) is used for the numerical determination of the equivalent sand roughness k_s of an arbitrary, three-dimensional, irregular surface roughness, such as it occurs for cast iron. The method is explained in detail and has been used in previous publications by the authors in Refs. (19, 24). Therefore, the method is explained briefly below:

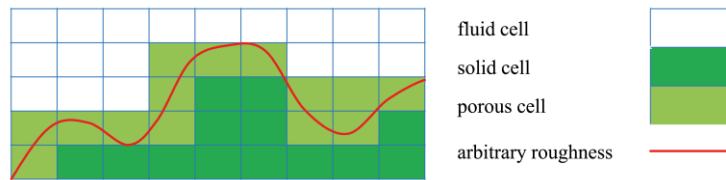


Figure 4: Cell definitions in the DPM. The figure is taken from Ref. (19).

Basically, a domain with one or multiple rough walls (e.g., a rough channel flow) is completely covered by a computational grid. In this grid, three cell types exist: fluid, solid and porous cells, see Figure 4. The fluid cells are in no contact with the roughness elements and the flow governing equations are solved, e.g., by the URANS equations {5}. The solid cells are completely covered by the roughness elements and these cells are cut-out in the preprocessing of the simulation. Thirdly, porous cells exist, which are partially filled by the roughness elements.

URANS equation in the fluid cells:

$$\frac{\partial \langle u_i \rangle}{\partial t} + \langle u_j \rangle \frac{\partial \langle u_i \rangle}{\partial x_j} = -\frac{1}{\rho} \frac{\partial p}{\partial x_i} + \nu \frac{\partial^2 \langle u_i \rangle}{\partial x_j^2} - \frac{\partial \langle u'_i u'_j \rangle}{\partial x_j} \quad \{5\}$$

URANS equation in the porous cells:

$$\frac{\partial \langle u_i \rangle}{\partial t} + \langle u_j \rangle \frac{\partial \langle u_i \rangle}{\partial x_j} = -\frac{1}{\rho} \frac{\partial p}{\partial x_i} + \nu \frac{\partial^2 \langle u_i \rangle}{\partial x_j^2} - \frac{\partial \langle u'_i u'_j \rangle}{\partial x_j} + \frac{1}{\rho} S_i \quad \{6\}$$

In the governing equations of the porous cells {6}, a sink S_i is included, which models the magnitude of pressure drop due to the non-resolved roughness elements. The pressure drop is formed by using dimensionless drag coefficient c_D . In the porous cells (for simplicity, we assume a flow around a roughness element with the constant width b in the following), the drag force of the cell is calculated and defined by:

$$F_D = \rho/2 c_D u_{cell}^2 A_{proj}, \quad \{7\}$$

where u_{cell} is the velocity in the cell and A_{proj} is the projected surface of the roughness element in the flow direction.

The definition of the surface A_{proj} is shown as an example in Figure 5 for a simple, regular roughness element. It is first assumed that the roughness fills the cell over the entire length of the cell Δx . To scale the influence of the roughness according to its height within the cell, the volume fraction α of the roughness is introduced.

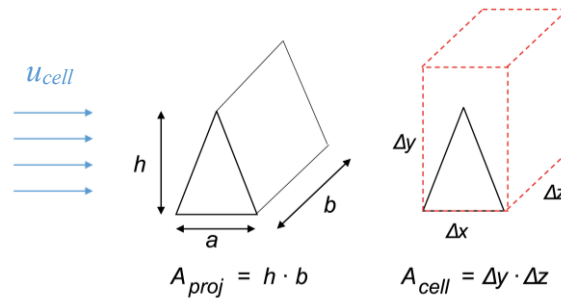


Figure 5: Exemplary calculation of the projected area A_{proj} for a regular roughness element in a porous cell. The figure is taken from Ref. (19).

$$\alpha = \frac{V_{roughness}}{V_{cell}} = \frac{A_{proj} \cdot a}{A_{cell} \cdot \Delta x} = \frac{A_{proj}}{A_{cell}} \quad \{8\}$$

In Equation (8), a and Δx are truncated since they are assumed to be equal. If Equation {8} is rearranged according to the projected area and substituted into Equation {7}, the drag force in a porous cell is obtained by:

$$F_D = \rho/2 c_D u_{cell}^2 A_{cell} \alpha. \quad \{9\}$$

If Equation {9} is normalized by the cell area, one gets:

$$\Delta p = \rho/2 c_D u_{cell}^2 \alpha. \quad \{10\}$$

To obtain the pressure gradient in flow direction accordingly, Equation {9} is then normalized over the length of the cell Δx , so that the following applies for the sink:

$$S = \frac{\Delta p}{\Delta x} = \rho/2 c_D u_{cell}^2 \frac{\alpha}{\Delta x}. \quad \{11\}$$

This sink was then implemented in the URANS equations {6} in the porous cells. Therefore, the sink was defined such that it accounts for a three-dimensional roughness element, which is placed in a three-dimensional boundary layer flow. The determination of the drag force c_D for every roughness element was realized by approximating the roughness structure in every cell as a 2D regular body, which drag force c_D was previously computed and stored in a database (comprehensively described in Ref. (19)).



Figure 7: Cast iron parts of the industrial pump.

Rough Channel Flow Simulations to Determine k_s for Cast Iron

Two cast iron surfaces were analyzed in this study. For this purpose, an industrial pump was cut (see Figure 7) and the surfaces at the impeller and the volute were digitized with a 3D-confocal microscope by the »Schweißtechnische Lehr- und Versuchsanstalt Mecklenburg-Vorpommern GmbH (SLV GmbH)«. Subsequently, the data were converted into point clouds. The scans have a dimension of $13 \times 13 \text{ mm}$ resp. $9 \times 13 \text{ mm}$, so that a sufficiently large area is available for the flow analysis with roughnesses. Figure 8 shows the scanned surfaces of the blades, and the volute and Table 1 summarizes some roughness topographical properties of these two surfaces.

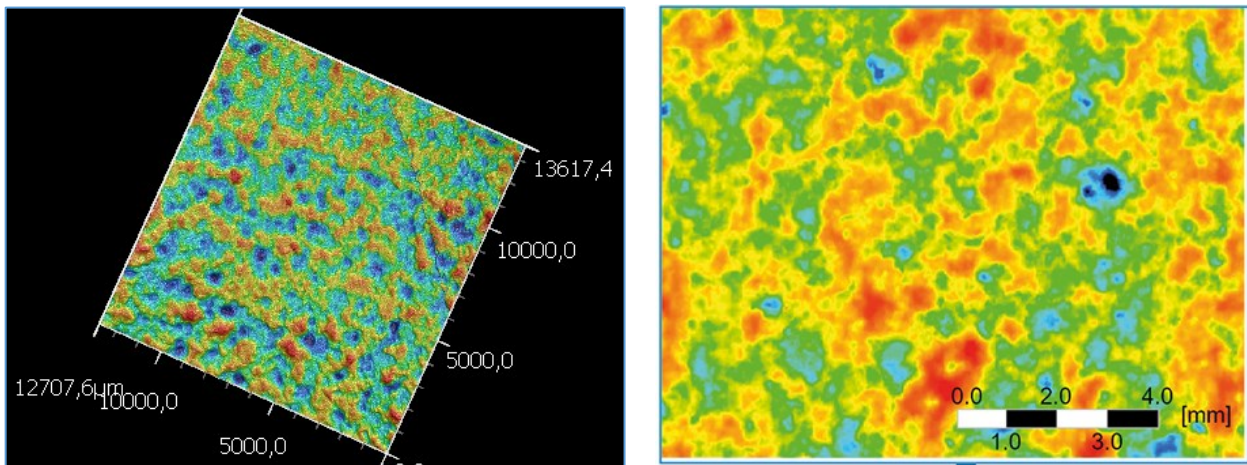


Figure 8: Left: Scan of the cast iron surface at the impeller (units in μm). Right: Scan of the cast iron surface in the volute. The red areas show the elevations, the blue areas show the valleys.

Table 1: Investigated roughness regions and some topographical roughness properties.

Region	Average roughness height k_a	Peak-to-trough roughness k_t
impeller	$13.5 \mu\text{m}$	$170 \mu\text{m}$
volute	$20.0 \mu\text{m}$	$280 \mu\text{m}$

Afterwards, channel flow simulations with the respective cast iron roughness at the bottom side were computed using *OpenFOAM 5.x* and the *pimpleFOAM* solver. A URANS approach with the $k-\omega$ -SST model was used to solve the governing equations {5} and {6} in the respective cell types. The boundary conditions were defined as shown in Figure 9. The flow was driven by a constant mass flow \dot{m} adjusted by a volume force (20), which corresponds to the investigated Reynolds number of $Re_H = u_b \cdot H/\nu = 400\,000$. At this Re_H , a fully rough behavior is present for the near-wall flow at the investigated cast iron surface (19).

The channel with the fluid cells and the roughness surface (solid and porous cells) was meshed using a cartesian, block-structured grid. Therefore, the grid was discretized by 248 elements in flow direction and 88 elements in the spanwise direction. The grid also contains 57 elements for the channel height, while a single cell resolves $1/5$ of the maximum roughness height k_t in the solid cell layer. A grid study and a validation regarding the rough channel's pressure losses at $Re_H = 100,000$ indicated in Ref. (19) that this grid size of $1.2 M$ elements is appropriate for the DPM simulations. Based on these simulations, the velocity downshift (exemplary shown in Figure 3) of the flow over the respective cast iron surface was determined. Using these downshift Δu^+ , the equivalent sand grain roughness k_s was calculated by Equation {2} and Equation {12} from Ref. (21).

$$\Delta u^+ = 1/\kappa \ln(k_s^+) + B - 8.5 \quad \{12\}$$

Please note that Equation {12} is only valid in the fully rough flow regime (which is fulfilled with our channel Reynolds number $Re_H = 400,000$).

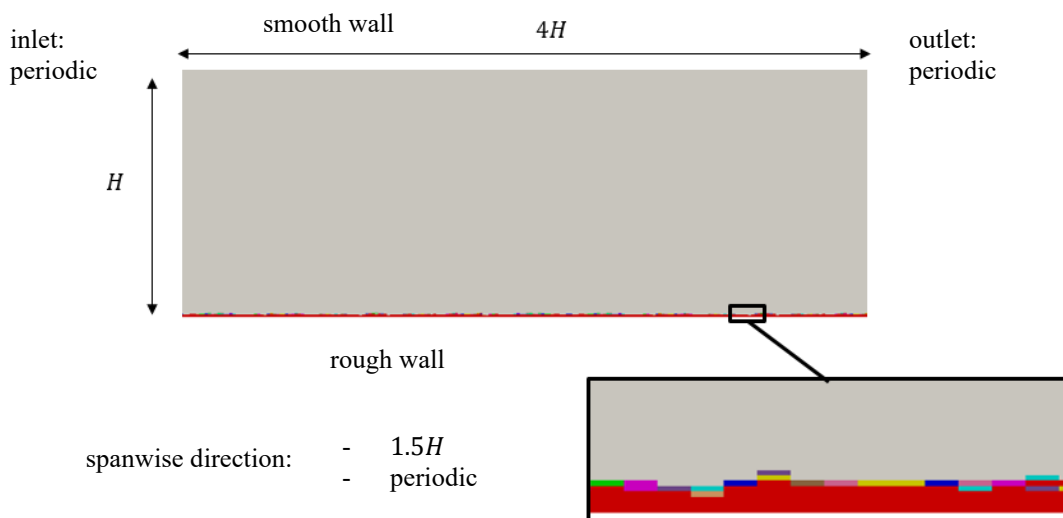


Figure 9: Sketch of the flow domain and boundary conditions of the rough channel flow simulations. The rough wall is at the bottom side. The gray area contains fluid cells, and the red area involves solid cells (which are cut out). The porous cells are highlighted in color in the figure. Each color reflects a specific c_D -value, which is used to model the roughness influence in these cells in form of a pressure drop, Equation {11}.

Turbopump Simulations with Zonal Roughnesses

After k_s was determined for the two cast iron surfaces from the DPM simulations, these k_s -values were specified at the rough walls in a turbopump simulation to numerically model the zonal roughness effects on the pump characteristics. The roughness modelling in CFX is described comprehensively in Ref. (6). The pump under investigation is a radial turbo pump with a $n_q = 13.4$ 1/min. The pump's design was adopted from an industrial pump and the meridional cut with the investigated roughness regions is shown in Figure 11.

URANS computations for this pump were carried out using *ANSYS CFX 2021 R1* (ANSYS Inc., Canonsberg, USA). A computational grid of $25.1 M$ grid elements was used with grid angles larger than 23° and an area-averaged wall distance of $y^+ = 1$ (for smooth walls) for all boundary layers. A High-Resolution spatial discretization and a 2nd order backward temporal discretization scheme were used. The $k-\omega$ -SST model (22) with curvature correction (23) was used for closure. At the outlet of the domain, a constant flow rate was specified, covering flow rates of $Q = (46; 65; 85; 93)$ m³/h. Furthermore, a zero relative static pressure and a zero gradient turbulence was defined at the inlet suction pipe. The transient rotor-stator method was used to couple the rotating and stationary domains

with a time step equal to a 1.5° rotation of the impeller (rotational speed of $n = 1450$ 1/min). Every simulation was performed for ten impeller revolutions and time-averaging was done for the last revolution.

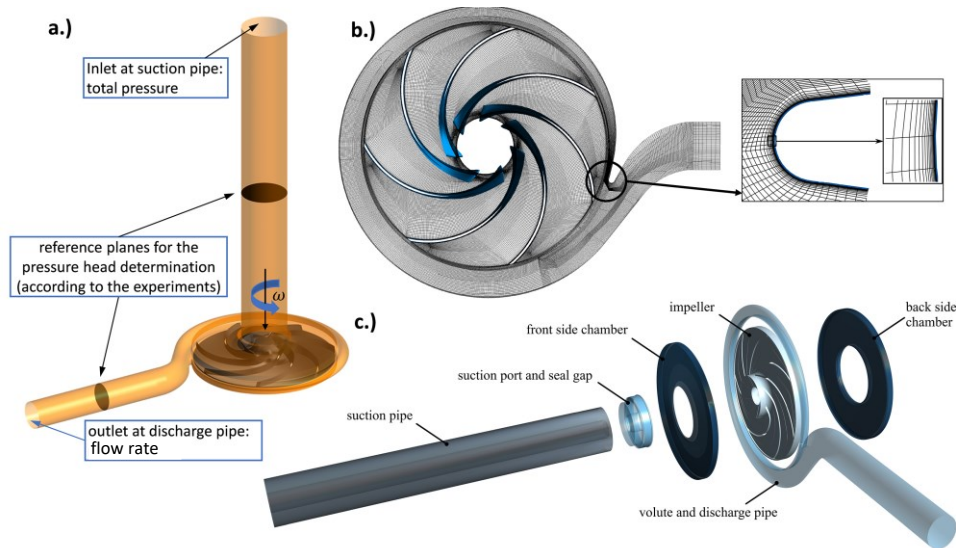


Figure 10: Model of the turbopump. a.) 3D model of the domain with the inlet and outlet BC. b.) Mesh in the impeller and volute region with a detailed view of the grid around the volute tongue. c.) Turbopump domain in an exploded view.

The simulation evaluation was performed in **three steps**:

Step 1.) Pump simulations with hydraulically smooth walls were conducted along the performance curve as a foundation to analyze the effect of roughness on the pump performance in the next steps. Furthermore, these simulations were also validated by experiments.

Step 2.) Pump simulations were performed with a defined roughness value of $k_s \approx 175 \mu\text{m}$ at the volute and the front side chamber of the pump (orange lines in Figure 11). This k_s -value was determined by the DPM simulations with the scanned cast iron surface from the volute. In the pump simulations, however, not only the volute was covered with roughness, but also the front side chamber. Juckelandt (3) found out that most of the losses due to roughness occur in these two regions. Therefore, an analysis of the roughness effect in these regions seems to be most useful. A validation of the pump characteristics for the rough pump simulations was also performed (experiments explained in Ref. (19)).

Step 3.) The rough pump simulations from Step 2.) were extended to account for the roughness in the impeller. Therefore, a value of $k_s \approx 90 \mu\text{m}$ was additionally specified at the impeller blades (red area in Figure 11). This roughness value was determined by DPM simulation performed with the cast iron roughness scanned in the impeller.

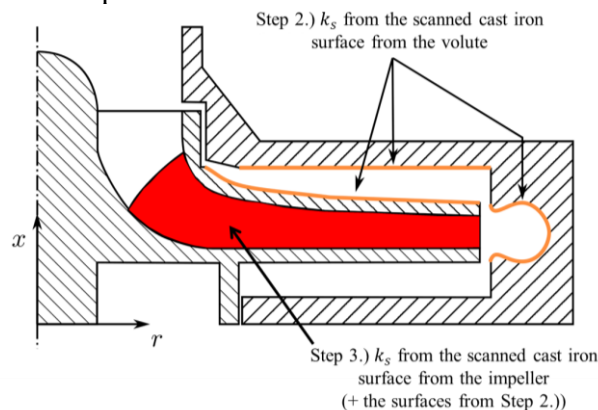


Figure 11: Meridional cut through the impeller, the side chambers, and the volute of the investigated pump. The areas where the k_s -values were defined in the pump simulations are highlighted in this figure.

RESULTS AND DISCUSSION

Determination of k_s using the DPM channel flow simulations

The velocity downshifts Δu^+ due to the rough surfaces were determined with the help of DPM simulations in the rough channel at $Re_H = 400,000$. Figure 12 displays this downshift for both cast iron surfaces. As already could be anticipated from the topographical roughness properties in Table 1, the roughness effect in the flow is stronger with the roughness scanned at the volute. Nonetheless, both simulations indicate a noticeable velocity downshift of $\Delta u^+ = 7.0$ for the cast iron surface at the impeller and $\Delta u^+ = 8.9$ for the cast iron surface in the volute. The sand grain roughness k_s was then determined using Equation {12} and its dimensionless and dimensioned value is specified in Table 2.

Table 2: Dimensioned and dimensionless equivalent sand grain roughness for the cast iron surfaces at the impeller and the volute.

Region	Sand Grain Roughness k_s	Dimensionless k_s (k_s^+)
impeller	89 μm	74
volute	177 μm	161

The dimensionless sand grain roughnesses have values greater than $k_s^+ > 70$ for $Re_H = 400\,000$, indicating that a fully rough regime is present in both simulations (17). This condition is needed to apply equation {12}, by which ultimately the dimensioned sand grain roughness was calculated. These sand grain roughnesses are in a range between (90 – 175) μm for cast iron depending on where the roughness surface was scanned in the pump. Compared to literature values for cast iron, these values are near the lower value of the uncertainty range from Ref. (14), which stated $k_s = 260\ \mu\text{m} \pm 50\%$ for cast iron. Nonetheless, this literature value as well as the others from Refs. (1,11–13) indicating a huge possible range of k_s for cast iron, which demonstrate the advantage of our DPM simulation in determining k_s specifically for an individual surface of interest.

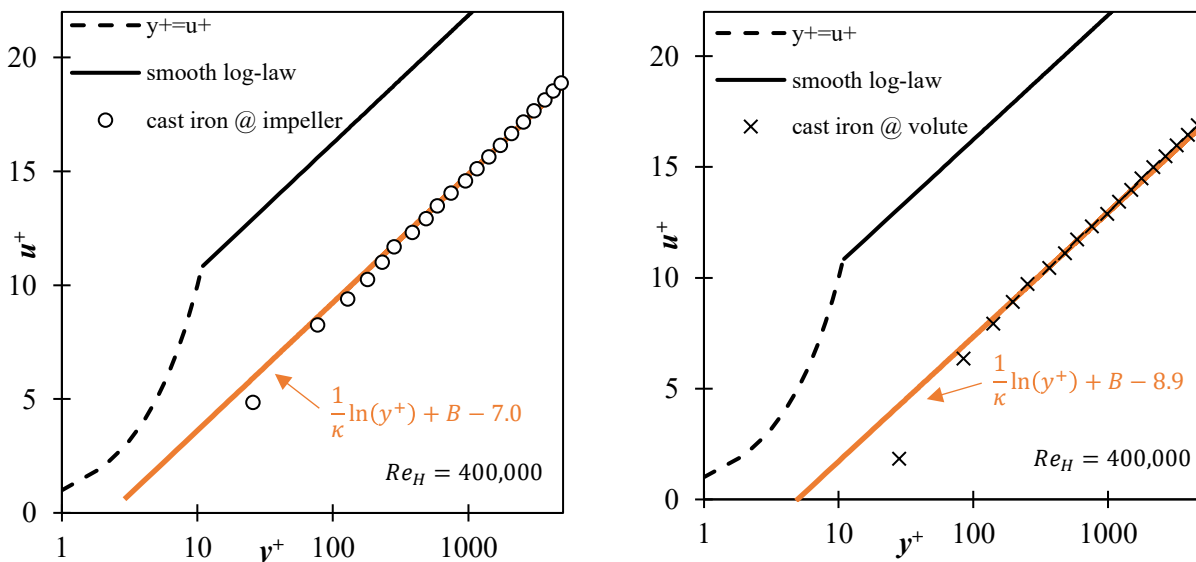


Figure 12: Velocity profiles in the rough channel flow simulations computed by DPM. Left: Simulation with the cast iron surface in the impeller. Right: Simulation with the cast iron surface in the volute.

Validation of the Smooth and Rough Turbopump Simulations

Table 3 summarizes the pressure heads H_p of the turbopump simulation with smooth and rough walls in the volute and the front side chamber. H_p was validated for every operation point to investigate, a.) if the flow simulation can reflect the experimental pressure heads in general, and b.) if the roughness modelling with the specified k_s -values works properly for our turbopump simulations. As can be seen from that table, the pressure heads are in an excellent agreement between experimentally and numerically assessed data with a maximal deviation of 3.5%.

Table 3: Pressure heads of the turbopump simulations with smooth and rough walls at the volute and the front side chamber in comparison with experimental values. The measurement uncertainties of the heads were less than 1% of the mean values.

Flow rate Q	Pressure head H_p with smooth walls [Step 1.]			Pressure head H_p with rough walls [Step 2.]		
	EXP	CFD	Rel. Dev.	EXP	CFD	Rel. Dev.
46 m ³ /h	39.9 m	40.4 m	+1.5 %	37.4 m	36.3 m	-2.9 %
65 m ³ /h	37.0 m	37.5 m	+1.4 %	33.9 m	33.3 m	-1.8 %
85 m ³ /h	31.5 m	32.6 m	+3.5 %	28.2 m	28.3 m	+0.4 %
93 m ³ /h	28.5 m	29.5 m	+3.5 %	25.1 m	24.7 m	-1.6 %

Influence of Zonal Roughnesses on the Pump Characteristics of a Turbopump

The pressure head and efficiency curves of the turbopump simulations with and without wall roughness in the volute and front side chamber are presented in Figure 13. A huge roughness effect on the pump characteristics can be seen in pressure head as well as in efficiency. The pressure head is decreased by $\Delta H_p \approx -4$ m and the efficiency by $\Delta \eta_i \approx -12$ % along the whole operating range. Juckelandt (5) justified this severe decrease in efficiency η_i in his study by an increase in torque M due to increased wall shear stresses τ_w at the front shroud in the front side chamber. The connection between efficiency, torque and wall shear stress is given in Equations {13} and {14}.

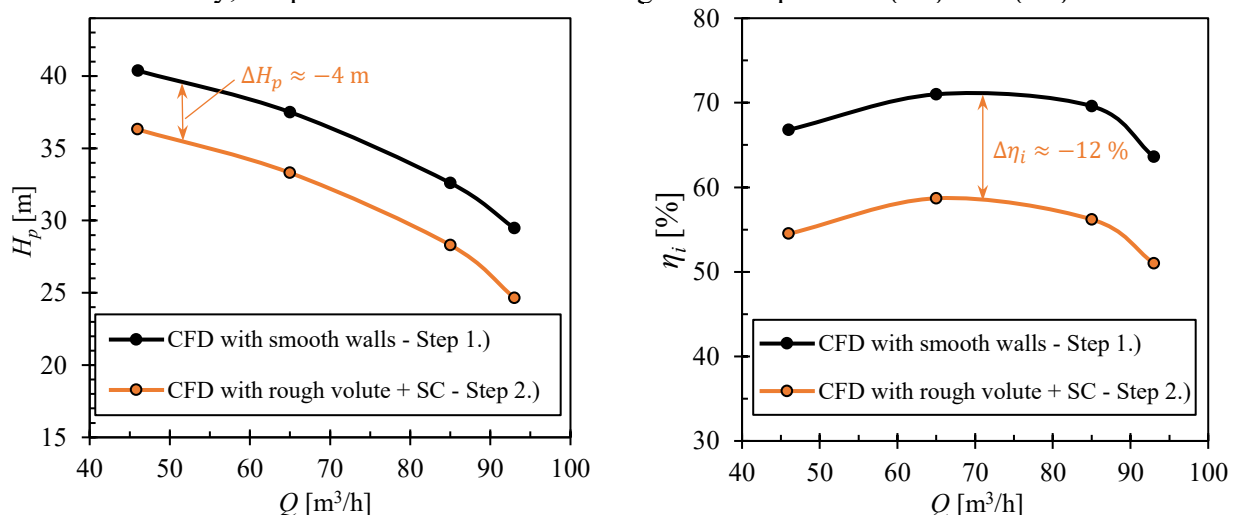


Figure 13: Comparison of the pump characteristics of turbopump simulations with smooth and with rough walls in the volute and the front side chamber. Please note: Compared to the CFD results in Figure 2, a low-Reynolds-number method was applied for the boundary layer treatment in this study's simulations.

$$\mathbf{M} = \left[\int_A \mathbf{r}_A \times (n_A p dA) + \int_A \mathbf{r}_A \times (t_A \boldsymbol{\tau}_w dA) \right] \cdot \mathbf{e}_z \quad \{13\}$$

$$\eta_i = \frac{\Delta p_t \cdot Q}{M \cdot 2\pi n} \quad \{14\}$$

Regarding the previously stated, Figure 14 show the wall shear stresses at the casing of the side chamber and the volute's wall. A significant increase in τ_w can be seen from smooth to rough flow case. These higher shear stresses (which are also present at the front shroud in the front side chamber) lead to the increased torque M and hence, to the significantly decreased η_i .

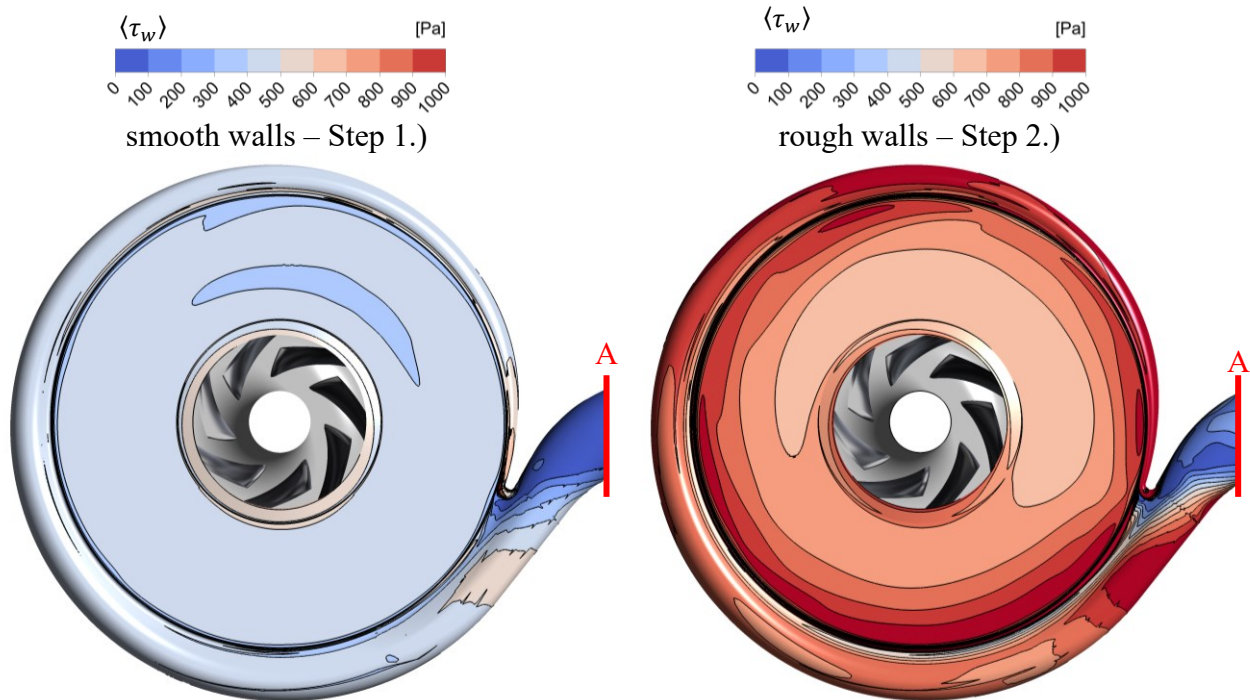


Figure 14: Comparison of the time-averaged wall shear stresses τ_w at the front side chamber and the volute between the turbopump simulations with smooth and rough walls at $Q = 65 \text{ m}^3/\text{h}$

Furthermore, the decrease in pressure head can also be attributed to the increased wall shear stresses in the volute and side chambers, which cause additional friction and hence, pressure losses. This can be seen from Table 4, where the static pressure head is shown for the outlet of the impeller and outlet of the outflow diffuser in the volute. It is noticeable from this table that the pressures at the impeller outlet are similar for the smooth and rough case but differ significantly when the flow passes through the pump regions, where wall roughness occurs.

Table 4: Progression of (static) pressure in the impeller and volute region. Comparison between the simulations with smooth and rough walls at $Q = 65 \text{ m}^3/\text{h}$.

mass-flow averaged static pressure head H_s	CFD with smooth walls – Step 1.)	CFD with rough walls – Step 2.)	Deviation
at outlet of impeller	27.2 m	27.0 m	$\Delta H_s = 0.2 \text{ m}$
in the volute behind the outflow diffuser (A in Figure 14)	35.2 m	31.1 m	$\Delta H_s = 4.1 \text{ m}$

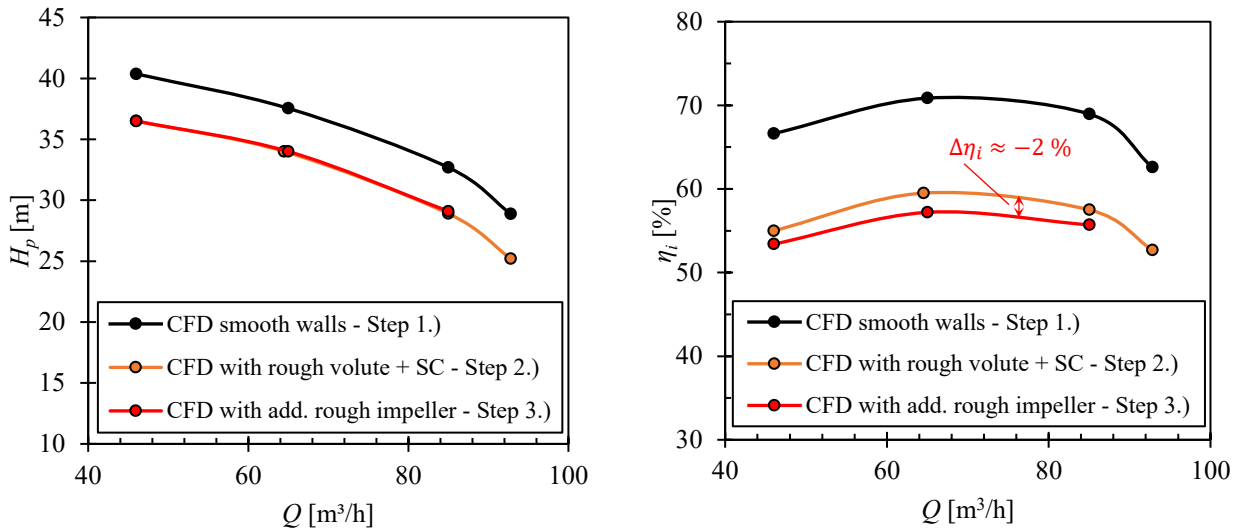


Figure 15: Comparison of the simulated pump characteristics with smooth (black line), with rough walls in the volute and the front side chamber (orange line), and with roughness in the volute, front side chamber and impeller (red line).

Figure 15 shows the pump characteristics between the simulations with roughness in the volute and front side chamber [Step 2.), $k_s = 175 \mu\text{m}$] and the simulation with additional roughness in the impeller [Step 3.), $k_s = 90 \mu\text{m}$]. As can be seen in the pressure head curve, the increase in pressure via the pump is not affected by the additional roughness in the impeller. This is also confirmed by the (static) pressure contours via the impeller (displayed in Figure 16), which indicate a similar pressure progression between the two rough simulations. However, Figure 15 also indicates a constant downshift in efficiency of $\Delta\eta_i \approx -2\%$ along the whole efficiency curve due to the additional roughness. This decrease in efficiency can again be explained by the higher wall shear stresses τ_w at the impeller blades, which are also shown in Figure 16. Due to the increased shear stresses at the blades, the impeller torque M increases (according to Equation {13}), which reduces η_i . Nonetheless, the roughness effect in the impeller is not as dominant as the roughness effect from the volute and side chamber. This is consistent with findings in Refs. (3,5), where it was highlighted that the greatest amount of losses (ca. 65%) in a radial pump with low n_q origin from the flow in the front side chamber and the volute.

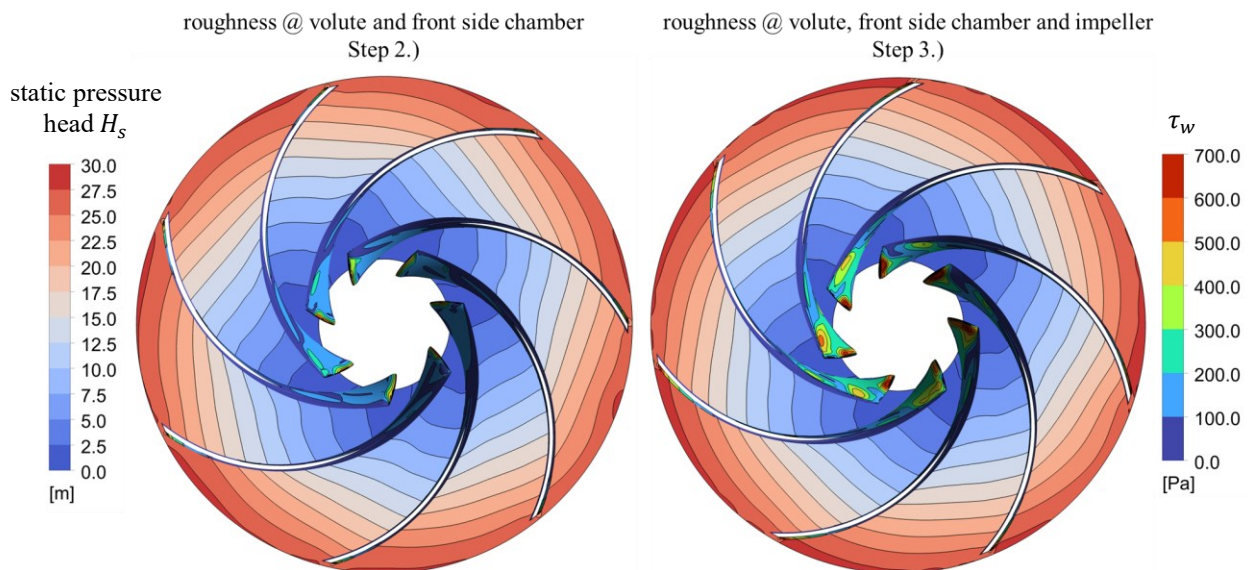


Figure 16: Comparison of the instantaneous (static) pressure increase in the impeller between the two rough flow simulations at $Q = 65 \text{ m}^3/\text{h}$ in a plan view. Also, the instantaneous wall shear stresses τ_w are plotted at the impeller blades.

SUMMARY AND CONCLUSION

The current study aimed to investigate the influence of zonal wall roughness on the pump characteristics in a radial turbopump with low specific speed. Therefore, the cast iron surface at the volute and the impeller were scanned and digitized, and its equivalent sand grain roughnesses k_s were determined with the help of rough channel flow simulations and our *discrete porosity method (DPM)*. Then, the two k_s -values were defined at the volute and front side chamber (k_s from volute), and at the impeller (k_s from impeller) in various flow simulations in a radial turbopump with low specific speed. When comparing the pressure head and efficiency between the simulations with smooth and rough walls in the volute and side chambers, a significant decrease in head and efficiency was identified. These decreases can be attributed to remarkably higher wall shear stresses at the rough walls. Also, the roughness at the impeller lead to a decrease in efficiency in all cases but was not as prominent as the effect due to the roughnesses in the volute and the side chamber.

In conclusion, this study shows the importance of considering zonal roughness effects in turbopump simulations with low specific speeds. Even though the roughness effect is not dominant in every component of a turbopump, the correct roughness modeling (by defining the correct k_s -value) should be applied in the high loss regions of a pump simulation. Only then, the correct pump characteristics can be numerically determined and turbopump designers can trust their design simulations and reduce costly experimental prototyping.

In the future, we will use the DPM to determine k_s in more rough regions (rear shroud, rear side chamber, sealing gaps, pipes) in the turbopump to analyze the influence of zonal roughnesses on the pump's flow more deeply. Furthermore, it would be interesting to analyze if modifications of the pump geometry can positively affect the head and efficiency of the rough pump.

ACKNOWLEDGEMENTS

This work was financially supported by the AiF in the framework of Industrial Collective 531 Research (IGF, project 19024 BR/1) and by the Forschungskuratorium Maschinenbau e.V. (project 5327038900)

REFERENCES

1. Gülich J. F., (2016). *Centrifugal Pumps*. 3rd ed. Berlin, Heidelberg, s.l.: Springer Berlin Heidelberg 2014.
2. Hallier S., Torner B., Kumar J., Wurm F.-H. (2016). *Miniaturization of an implantable pump for heart support*. 16th International Symposium on Transport Phenomena and Dynamics of Rotating Machinery, Honolulu, USA. Available at <https://hal.inria.fr/ISRROMAC2016> Accessed March 09, 2023.
3. Juckelandt K., Bleeck S., Wurm F.-H. (2015). *Analysis of Losses in Centrifugal Pumps with Low Specific Speed with Smooth and Rough Walls*. In: Martelli F, Díaz RV, eds. Proceedings of the 11th European Conference on Turbomachinery 2015; 1-10.
4. Juckelandt K., Wurm F.-H. (2015). *Applicability of Wall-Function Approach in Simulations of Turbomachines*. In: ASME, ed. Proceedings of the ASME Turbo Expo 2015: Turbine Technical Conference and Exposition-2015. New York, N.Y.: ASME; 1-10.
5. Juckelandt K. (2017). *Experimentelle und numerische Untersuchung der Strömung in Pumpen kleiner spezifischer Drehzahl unter Berücksichtigung des Rauheitseinflusses*. [PhD Thesis]. Rostock: Universität Rostock.
6. Lechner R., Menter F. R. (2004). *Development of a rough wall boundary condition for omega-based turbulence models: TR-04-04, Rough Walls*. Report, ANSYS CFX.

7. Apsley D. (2007). *CFD Calculation of Turbulent Flow with Arbitrary Wall Roughness*. Flow Turbulence Combust. 78(2):153-175.
8. Aupoix B. (2014). *Wall Roughness Modelling with k - ω SST Model*. In: ERCOFTAC, ed. 10th International ERCOFTAC Symposium on Engineering Turbulence Modelling and Measurements: Springer.
9. Wilcox D. C. (2008). *Formulation of the k - ω Turbulence Model Revisited*. AIAA Journal, 46(11):2823-2838.
10. Knopp T., Eisfeld B., Calvo J. B. (2009). *A new extension for k -turbulence models to account for wall roughness*. International Journal of Heat and Fluid Flow, 30(1):54-65.
11. Wagner W (2008). *Strömung und Druckverlust*. 6th ed. Würzburg: Vogel.
12. Fried E., Idelcik I. E. (1997). *Flow resistance: A design guide for engineers*. [reprint]. Philadelphia, PA: Taylor & Francis.
13. Oertel jr. H., Böhle M., Dohrmann U. (2009). *Strömungsmechanik: Grundlagen – Grundgleichungen – Lösungsmethoden – Softwarebeispiele*. 5th ed. Wiesbaden: Vieweg + Teubner.
14. White F. M. (1998). *Fluid Mechanics*. 4th ed. Boston: McGraw-Hill.
15. Nikuradse J. (1933). *Strömungsgesetze in rauhen Rohren*. VDI-Forschungsheft, 4.
16. Schlichting H. (1936). *Experimentelle Untersuchungen zum Rauheitsproblem*. Ing. Arch, 7(1):1-34.
17. Schlichting H., Gersten K. (2006) *Grenzschicht-Theorie*. 10th ed. Berlin, Heidelberg: Springer Berlin, Heidelberg.
18. Flack K. A., Schultz M. P. (2010). *Review of Hydraulic Roughness Scales in the Fully Rough Regime*. Journal of Fluids Engineering, 132(4):41203.
19. Torner B., Duong D., Wurm F.-H. (2023). *Numerical Determination of the Equivalent Sand Grain Roughness of a Turbopump's Surface and its Roughness Influence on the Pump Characteristics*. International Journal of Turbomachinery, Propulsion and Power, 8(1):5.
20. Fröhlich J. (2006). *Large Eddy Simulation turbulenter Strömungen*. 1st ed. Wiesbaden: Teubner.
21. Schultz M. P., Flack K. A. (2009). *Turbulent boundary layers on a systematically varied rough wall*. Phys. Fluids, 21(1).
22. Menter F. R. (1993). *Zonal Two-equation k - ω turbulence Models for Aerodynamic Flows*. AIAA Journal, 2906.
23. Smirnov P.E., Menter F.R. (2009). *Sensitization of the SST Turbulence Model to Rotation and Curvature by Applying the Spalart–Shur Correction Term*. J. Turbomach, 131(4).
24. Malchow S., Wurm F.-H., Torner B. (2023). *Numerical Determination of the Equivalent Sand Roughness for a Regular Surface Roughness (Cubes)*. In: Proceedings Topical Problems of Fluid Mechanics 2023, Prague, Edited by David Šimurda and Tomáš Bodnár, pp. 129.